

The Color-Magnitude Relation in Coma: Clues to the Age and Metallicity of Cluster Populations

Andrew Odell

Department of Physics and Astronomy, Northern Arizona University, Box 6010, Flagstaff, AZ 86011;
andy.odell@nau.edu

James Schombert

Department of Physics, University of Oregon, Eugene, OR 97403; js@abyss.uoregon.edu

Karl Rakos

Institute for Astronomy, University of Vienna, A-1180, Wien, Austria; karl.rakos@chello.at

ABSTRACT

We have observed three fields of the Coma cluster of galaxies with a narrow band (modified Strömrgren) filter system. Observed galaxies include 31 in the vicinity of NGC 4889, 48 near NGC 4874, and 60 near NGC 4839 complete to $M_{5500} = -18$ in all three subclusters. Spectrophotometric classification finds all three subclusters of Coma to be dominated by red, E type (ellipticals/S0's) galaxies with a mean blue fraction, f_B , of 0.10. The blue fraction increases to fainter luminosities, possible remnants of dwarf starburst population or the effects of dynamical friction removing bright, blue galaxies from the cluster population by mergers. We find the color-magnitude (CM) relation to be well defined and linear over the range of $M_{5500} = -13$ to -22 . The observational error is lower than the true scatter around the CM relation indicating that galaxies achieve their final positions in the mass-metallicity plane by stochastic processes. After calibration to multi-metallicity models, bright ellipticals are found to have luminosity weighted mean $[\text{Fe}/\text{H}]$ values between -0.5 and $+0.5$, whereas low luminosity ellipticals have $[\text{Fe}/\text{H}]$ values ranging from -2 to solar. The lack of CM relation in our continuum color suggests that a systematic age effect cancels the metallicity effects in this bandpass. This is confirmed with our age index ($\Delta(bz - yz)$) which finds a weak correlation between luminosity and mean stellar age in ellipticals such that the stellar populations of bright ellipticals are 2 to 3 Gyrs younger than low luminosity ellipticals. With respect to environmental effects, there is a slight decreasing metallicity gradient with respect to distance to each subcluster center, strongest around NGC 4874. Since NGC 4874 is the dynamic and x-ray center of the Coma cluster, this implies that environmental effects on low luminosity ellipticals are strongest at the cluster core compared to outlying subgroups.

Subject headings: galaxies: evolution — galaxies: stellar content — galaxies: elliptical

1. INTRODUCTION

The age and star formation history of elliptical galaxies are, of course, key tests to our understanding of galaxy evolution processes. Our early notions that ellipticals are old objects forming their stars at high redshift in a single episode has come into question by HST examination of nearby dwarf galaxies (see review by Grebel 1998). Detailed CMD's indicate several episodes of star formation in dwarf galaxies, some within

a few Gyrs of the present. The detection of Balmer lines (Caldwell *et al.* 1993) and the high fraction of blue galaxies in distant clusters (Rakos & Schombert 1995) both challenge the monolithic collapse scenario for ellipticals.

Observations of ellipticals from dwarf to giant in a range of environments is the first step in resolving various predictions from hierarchical models of galaxy formation. In recent years, several spectroscopic programs have determined the age and metallicity of Coma and Fornax galaxies through the use of such indices as Mg_2 and $H\beta$ (Trager *et al.* 2000, Kuntschner *et al.* 2001, Terlevich & Forbes 2001, Poggianti *et al.* 2001). Spectroscopic studies are, of course, superior to determining metallicity values directly from atomic lines. While some comparison to models is required to interpret the spectral age indicators, there are several independent estimators of both age and metallicity.

An alternative approach is our narrow band photometry method, which focuses on the shape of a galaxy’s integrated spectral energy distribution (SED) by way of near-UV and blue colors. This has the advantage of measuring the behavior of the stellar population as it reflects the temperature of the red giant branch and turnoff points, but has the disadvantage of being very model dependent since the red giant branch (RGB) must be broad even in ellipticals and requires some estimation of the luminosity weighted contribution from different metallicity populations (multi-metallicity models). In our most recent paper using the generalized Strömrgren filter system (Rakos *et al.* 2001), the possibility was explored of using various color indices as age and metallicity estimators for ellipticals. The integrated colors of Galactic globular clusters, with known ages and metallicities, were used to demonstrate and calibrate our narrow band system for single generation objects. Multi-metallicity models were derived from the globular cluster (GC) calibration and compared to the colors of dwarf ellipticals in Fornax. While we have been successful at predicting the global characteristics of ellipticals in clusters, such as slope of the color-metallicity relation, with our simple multi-metallicity models, our methods are by no means superior to spectroscopic survey but, in fact, serve as a complement to their programs. In general, spectral investigations are superior in the detailed information they provide, but the goal here is to develop a system that can be used for low brightness objects or distant (i.e. faint) clusters where spectroscopy is very impractical.

In an attempt to confirm and extend the Fornax results, we have carried out photometry of three separate regions of the Abell cluster A1656 (Coma) as a first step in the investigation of the behavior of low luminosity ellipticals and dwarf galaxies in clusters of galaxies with increasing redshift. We have selected Coma because it is the nearest rich cluster (richness class 2) with a dynamically evolved galaxy distribution (Bautz-Morgan type II). Coma is one of the most studied clusters in the sky, and has long been regarded as the prototypical relaxed massive cluster of galaxies. However, recent studies of Coma have suggested that the cluster is the product of a recent and an ongoing cluster-group merger. While the bright galaxies in Coma are well understood, the distribution and history of faint cluster galaxies has not yet been fully investigated. In addition, there has been a renewal of interest in the galaxy luminosity function in rich clusters, in particular at its faint end. It is assumed that low-luminosity galaxies and their evolution almost certainly play an important cosmological role in explaining the large numbers of galaxies counted at faint magnitudes. Interest in the faint end of the luminosity function derives from the fact that low luminosity ellipticals and dwarf galaxies serve as key tests to our understanding of galaxy formation and evolution. For example, in hierarchical models, galaxies are constructed from mergers with smaller-mass dwarfs.

The goal of this paper is threefold. First, we will examine the cluster populations for the three regions in Coma around NGC 4889, 4874 and 4839 in terms of the spectrophotometric classifications. Two recent papers (Rakos, Odell & Schombert 1997 and Rakos, Dominis & Steindling 2001) have shown that the ratio of the number of blue to red galaxies in clusters (A2317 and A2218 respectively) has a strong dependence

on absolute magnitude, such that blue galaxies dominate at both the bright and faint end of the cluster luminosity function. We will examine if the same effect occurs in Coma, a present-day counterpart to these intermediate redshift clusters. Second, we will investigate the behavior of the color-magnitude (CM) relation for ellipticals. In particular, we will map the CM relation into our metallicity and age calibrations. Lastly, we will examine the radial dependence of age and metallicity for early-type galaxies around the three dominate galaxies to check for environmental influences on the star formation history of cluster galaxies.

2. OBSERVATIONS

2.1. Data Acquisition and Reduction

The Coma cluster (Abell 1656) is roughly 89 arcmins in radius, with three dominant galaxies (NGC 4889, NGC 4874 and NGC 4839) forming the core of three separate cluster components. The first two of these, only 7 arcmins apart, seem to be the relic central galaxies of previous groups that have recently merged into the current cluster. An additional subcluster, centered on the third galaxy NGC 4839 40 arcmins to the southwest, seems to be falling into the central region (Colles & Dunn, 1996), or has just passed through the main body of the cluster (Burns *et al.*, 1994), perhaps triggering new star formation (Caldwell & Rose, 1998).

Each section of the Coma cluster was observed with the Kuiper 1.55m Telescope of the Steward Observatory on Mt. Bigelow Arizona. Data was taken with the LPL Focal Reducer and 2K CCD chip (binned to 1K) which yielded 0.65 arc sec/pixel for a field size of 10.8 arcmin. We centered one field on NGC 4889 (April 2-4, 2000) and the other on the central giant NGC 4874 (May 10-11, 2000). Our results are restricted to these central regions and therefore are not necessary typical for the whole cluster. The total April exposure time for the *uz* filter was 11,700s, the *vz* filter 9,600s, the *bz* filter 3,000s and the *yz* filter 3,000s. Each set of exposures was divided in frames of 600s to 1200s to reduce the influence of cosmic rays and irregularities of pixels on the chip. For the May observing run, the total exposure times were 7,200s in each of *yz* and *bz* and 9600s in *vz*. Weather conditions restricted the *uz* filter to 2,400 seconds, and therefore it is of lower quality. Calibration was obtained through a number of spectrophotometric standards measured on each night. The region around NGC 4839 was observed with the 4-m Mayall telescope of the National Optical Astronomy Observatory on Kitt Peak Arizona (June 27-28, 2001). The Prime Focus T2KB CCD camera produces a 14 arcmin field with 0.42 arc sec/pixel. The total exposure of 1,800s in each filter consists of three 300s exposures each night.

The reduction procedures have been published in Rakos, Maindl & Schombert (1996) and references therein. The photometric system is based on the theoretical transmission curves of filters (which can be obtained from the authors) and the spectra of spectrophotometric standard stars published in the literature (Massey & Gronwall, 1990; Hamuy *et al.* 1994). The convolution of the transmission curves and the spectra of the standard stars produces theoretical flux values for color indices of the standard stars corrected for all light losses in the equipment and the specific sensitivity of the CCD camera. For distant clusters, the filters are shifted for the proper redshift of the galaxies. For Coma, the filters were at zero redshift and a small k-correction was made. The comparison with the calculated theoretical fluxes delivers the corrections, which are finally applied to the observed colors of galaxies with the same real filters. The disadvantage of the method is the need for a separate set of real filters for different redshifts of clusters. The main advantages of this observing technique are that the filters are designed to sample spectral regions which are very sensitive to changes in the underlying physical properties and that these filters avoid all strong emission lines, which

cause confusion in UBV photometry of active galaxies.

Magnitudes were measured on the co-added images using standard IRAF procedures and are based for brighter objects on metric apertures set at 32 kpc for cosmological parameters of $H_o = 75 \text{ km s}^{-1} \text{ Mpc}^{-1}$ and the Benchmark cosmology ($\Omega_m = 0.3, \Omega_\Lambda = 0.7$). For fainter objects the aperture has been adapted to deliver the best possible signal to noise ratio, but always using the same aperture for all four filters. Color indices are formed from the magnitudes: $uz - vz, bz - yz, vz - yz$, and $mz [= (vz - bz) - (bz - yz)]$. Foreground galactic reddening in the direction of Coma is negligible and was not taken into account. Typical observing errors were 0.03 mag in color at the bright end of the sample and 0.08 mag at the faint end. A total number of 415 objects were detected in all four filters. A majority are rejected as foreground stars or background galaxies based on our photometric criteria. Some faint objects are rejected for insufficient signal in all four passbands for accurate colors.

2.2. Cluster Membership

Cluster population statistics must deal with the contamination by stars as well as by foreground and background galaxies. Since our filters are chosen to correspond to the redshift of the cluster, we can use the colors to discriminate cluster membership in a very efficient manner. We calculated synthetic Strömgen colors for a compilation of approximately 150 spectra of nearby galaxies covering all possible morphological types. It has been demonstrated that galaxies observed in their rest frame Strömgen bands are confined to a very limited region of the three-dimensional color space subtended by the four bands (Steindling, Brosch & Rakos 2001). Since real galaxies were used as templates (and not models), we need not worry about different constituents of model galaxies. The efficiency of this rejection mechanism is characterized by the selected maximum deviation ‘sigma’ between any measured color from the same color of the best template galaxy. Note that our filters are narrow enough to obtain data of sufficient spectral resolution for identification and classification purposes, but sufficiently wide so that the cluster’s velocity dispersion does not affect the colors.

Membership for the Coma cluster is straightforward for the bright end since all galaxies down to $m_{5500} = 16.5$ have measured redshifts. This comprises 53 galaxies of the 139 in the total sample. Another 26 galaxies fainter than 16.5 have measured redshifts from various deeper surveys. For the remaining 60 galaxies, without redshifts, we assign membership based on their colors and morphological appearance (i.e. most of these galaxies are dE or dI systems, diffuse and low in surface brightness). We note that this sample is not complete in either magnitude or area. We have eliminated objects with poor photometry from the sample regardless of apparent magnitude. We are also focused on three fields surrounding NGC 4889, 4874 and 4839 with no attempt made to sample the outer region of the cluster. On the other hand, our sample has high reliability in the sense that each member of the sample has a strong probability of being a cluster member, and its spectrophotometric classification has a high degree of confidence by only using high accuracy data (see next section).

2.3. Spectrophotometric Classification

Once cluster membership has been established, the principal moment values can also be used to assign a spectrophotometric classification. This procedure is outlined in Steindling, Brosch & Rakos (2001); however, that project related photometric values with morphological appearance. For our goals, it is beneficial to relate the photometric values to a measure of current star formation rate rather than morphological type.

Although we find those photometric classifications will map into morphological ones such that passive, red systems will typically be E/S0 types and star-forming colors will typically be late-type spirals.

To this end, we have divided the first principal component axis (PC1) into four subdivisions; E (passive, red objects), S (star formation rates equivalent to a normal disk galaxy), S- (transition between E and S) and S+ (starburst objects). In addition, we can separate out objects with signatures of non-thermal continuum (AGN) under the categories of A+, A and A- to match their star forming colors. It is important to remember that these classifications are based solely on the principal components as given by the color indices from four filters. While, in general, these spectrophotometric classes map into morphological ones (i.e. E types are ellipticals, S- are S0 and early-type spirals, S are late-type spirals and S+ are irregulars), the system has merit as an independent measurement from morphology based on the color of the dominant stellar population in a galaxy. For Coma, some comparison to morphological types can be made. In all three subclusters, 72 of the galaxies have morphological types in the literature. Of these 72 morphological types, 63 are spectrophotometrically classified as E type. Within the 63 E types, 56 are classed as E/S0 morphologically. The remaining seven are classified as S0/a or Sa. Four S- type galaxies are S0's, two S galaxies are Sc's and 3 A types are E or S0's. Unfortunately, Coma offers a very limited range of morphological types; however, all the E types are early-type systems. The seven Sa galaxies classified as E type are not of concern since we use aperture magnitudes, which will heavily weight the large, red bulge in early-type spirals. Thus, regardless of the shape and appearance of a galaxy, its spectrophotometric classification is based on the luminosity weighted color of the underlying stellar population.

Following the membership procedure, Tables 1, 2 and 3 shows the final selection of 139 cluster members for the NGC 4889 group, NGC 4874 group and NGC 4839 group respectfully. Final selection included all objects with errors less than or equal to 0.08 mag. Tables 1, 2 and 3 list the position of the cluster objects (J2000), the observed colors and magnitudes (apparent and absolute). The derived quantities, described in the text, are $[\text{Fe}/\text{H}]$ and $\Delta(bz - yz)$ and the resulting galaxy class. Note that $[\text{Fe}/\text{H}]$ and $\Delta(bz - yz)$ are only calculated for E type systems as restricted by our model interpretations.

3. DISCUSSION

3.1. Characteristics of the Coma Cluster

The Coma cluster is our nearest example of a rich, compact, elliptical-rich system that is indicative of an evolved environment. For this reason, Coma also serves as a calibration for studies of rich distant clusters and comparison of those cluster populations with a present-day population. However, unlike a classic cD cluster with a single dominant elliptical at the bottom of the cluster potential surrounded by a population of lesser cluster members, Coma offers a somewhat more diverse cluster structure. The cluster core is dominated by two equally bright ellipticals NGC 4889 and NGC 4874. Both have separate populations that are visible in galaxy density diagrams (Geller & Beers 1982) and x-ray contours (Henry *et al.* 1981) centered on the ellipticals. In addition, Coma has a small subcluster to the southwest centered on NGC 4839. These three dynamically separate components contain a majority of the luminous material in Coma.

The central ellipticals for the three subsystems of Coma also present a diverse set of objects. NGC 4889 and NGC 4874 have similar total magnitudes (e.g. luminous mass), but differ in their structure. NGC 4874 is a classic cD galaxies with an extended envelope typical of that class of galaxies (Schombert 1987), whereas NGC 4889 is a D type elliptical which are noted for their diffuse structure but lacking the extended envelope of the cD class. Dynamical studies indicate the origin of the diffuse interior structure in D and cD

galaxies is due to past mergers of companion galaxies. The origin of the extended cD envelopes is due to cluster properties, as they relate to the ability for a cluster environment to strip cluster members to develop a cluster-sized envelope of stars that surrounds the central galaxy (Schombert 1988).

The Coma cluster provides a unique situation containing a cD galaxy, and its extended envelope (NGC 4874) paired with a D galaxy and its subpopulation (NGC 4889). In addition, the southwest subgroup of Coma centers on NGC 4839, itself an example of a low luminosity cD galaxy and an example that the extended envelope phenomenon is associated with the local cluster environment rather than the properties of the central dominant galaxy. Together the three subgroups within Coma provide a laboratory to investigate the star formation history of galaxies in a classic cD environment, a merger dominated D system and a small subcluster with evidence of stripping to produce a low luminosity cD system. We begin this investigation an examination of the luminosity function for each of these subclusters.

3.2. Luminosity Functions

The luminosity function of the Coma cluster has been well studied by numerous groups over many wavelengths (see Smith *et al.* 1997 for references). Due to the narrow width of our filter system, our data is not as deep in limiting magnitude as other surveys. However, there are sufficient numbers of galaxies to produce a luminosity function for the populations around each giant elliptical. Those values are shown for each subcluster in the top panel of Figure 1 as log counts (N) versus apparent magnitude (m_{5500}). The unusual brightness of the first ranked galaxy in each group is obvious in Figure 1. This is a well known phenomenon that supports the idea that first ranked ellipticals in rich clusters owe about half their luminosity to the past mergers of lesser cluster members (Schombert 1987). The luminosity functions of the NGC 4889 and NGC 4874 subclusters have similar shapes, but the NGC 4874 group has the denser concentration of galaxies, again indicating the fact that the potential well is deeper around NGC 4874 compared to NGC 4889. We note that the faint end of the luminosity function for the NGC 4839 group rises more sharply than the NGC 4889 or NGC 4874 groups. This perhaps signals a more advanced evolutionary state for the populations around NGC 4889 and NGC 4874 as dwarf galaxies are cannibalized to create their extended envelopes.

The bottom panel in Figure 1 displays the summed luminosity function for all three subclusters plus a single Schechter-type fit. Despite the limited number of galaxies we have measured, the luminosity function for each population shows the characteristic upturn at $m_{5500} = 17$ ($M_{5500} = -18$). Interestingly, most of the steepness at the faint end is due to NGC 4839 group; however, the general trend of a break in the luminosity function at $M = -19$ follows the results of previous studies (Smith *et al.* 1997, De Propris *et al.* 1995, Secker *et al.* 1997, Thompson & Gregory 1993 and Bernstein *et al.* 1995). The overall luminosity function can be better fit by two Schechter-type components, the bright end having the conventional $\alpha = 1$, and the low luminosity galaxies with a steeper $\alpha = 1.7$, similar to the characteristics of other rich clusters such as Shapley 8 (Metcalf *et al.* 1994). Since field surveys have demonstrated a shallow slope for the faint end ($\alpha = -1$, Ellis *et al.* 1996), our narrow band luminosity function confirms the richer dwarf population found in dense clusters. Certainly, the population near the bright galaxies in Coma is richer in low luminosity galaxies, as expected from dynamical friction arguments (Schombert 1988).

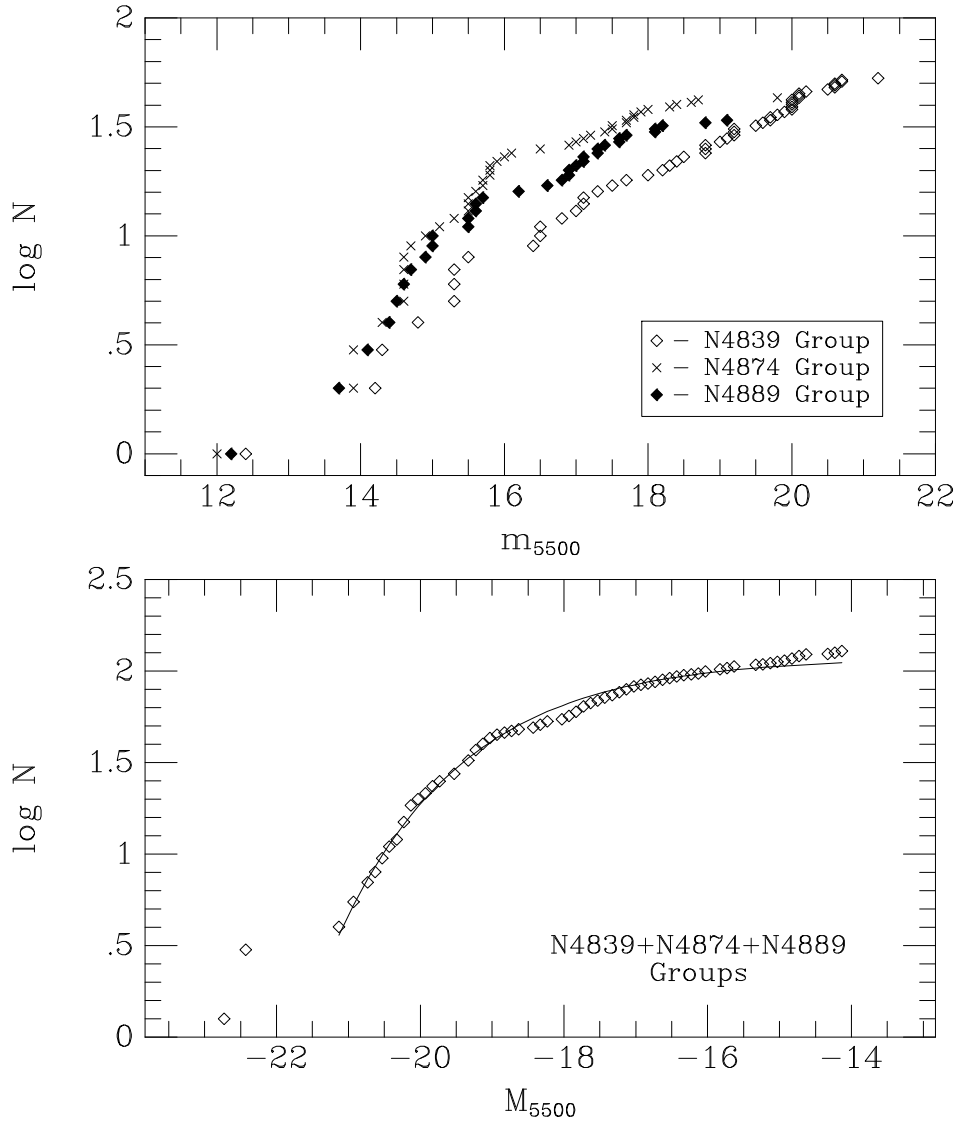


Fig. 1.— The luminosity function for the three subclusters in Coma. The top panel displays the data for the individual subclusters, the bottom panel is the summed population along with a best fit Schechter-type function. The total population shows the characteristic upturn at $m_{5500} = 17$ ($M_{5500} = -18$) with a the bright fit of $\alpha = 1$ and the low luminosity galaxies with a steeper $\alpha = 1.7$.

3.3. Butcher-Oemler Effect

The signature test of galaxy evolution in cluster populations is the Butcher-Oemler effect, the fraction of blue to red galaxies as a function of redshift. Being a photometric selection process, our classification scheme makes for an obvious comparison to the Butcher-Oemler fraction. In this context, the population fractions, as defined by our spectrophotometric criteria, are fairly typical of a low-redshift cluster. For the total cluster, we find that 71% of the cluster members are E type (see Table 4), which covers a majority of the galaxies that would be classified as E or S0 morphologically. In comparison, for a rich cluster we expect the ratio E:S0:Sp+Irr would be 20%:40%:40% (Oemler 1992), slightly more spiral-rich than our values. However, we note our measurements are restricted to the central part of the three densest subclusters and we would expect a larger number of E/S0 galaxies in comparison to spirals due to the density-morphology effect. Table 4 presents the population fractions for the three subclusters.

The photometric change in cluster populations is measured by the fraction of blue galaxies, f_B . The original broadband definition of blue galaxies f_B given by Butcher & Oemler (1984), is the ratio of galaxies 0.2 mag bluer than the mean color of the E/S0 sequence (after k-corrections) to the total number of galaxies in the cluster. As discussed in Rakos, Schombert & Kreidl (1991), we have defined the fraction of blue galaxies as the ratio of the number of galaxies bluer than $bz - yz = 0.22$ to the total number of galaxies, effectively the same prescription when accounting for filter central wavelengths as the original Butcher & Oemler definition. The relevant values of f_B for each subcluster are found in Table 4 as the number of blue galaxies. The NGC 4889 group has the highest number of blue galaxies (16%) with the NGC 4874 group with the least (2%) and the NGC 4839 group in between (13%). The NGC 4839 data is slightly deeper in limiting magnitude, but selecting brighter cutoff limits does not change the integrated f_B values. It is notable that both NGC 4874 and NGC 4839 have cD envelopes providing circumstantial evidence that dynamical environment effects are much stronger in those subclusters than the NGC 4889 group. The total f_B value for the dense regions of Coma is 0.10, a fairly standard value for nearby rich clusters (Oemler 1992).

The top panel in Figure 2 displays the cumulative behavior of f_B with luminosity for each of the three subclusters and the sum of the sample. As is typical for rich clusters, the top of the luminosity function is completely dominated by red, early-type galaxies (ellipticals and S0's). As the luminosity drops below -18 we find a rise of f_B due to the increasing contribution from blue, low-mass galaxies. Figure 2 is the best example of how the interpretation of the blue fraction in clusters is dependent on the completeness of observations with respect to cluster boundaries and the photometric limiting magnitude since the f_B values do not stabilize until $M_{5500} = -15$. This plateau is reached in each of the various subclusters even though their final f_B values vary from 0.14 to 0.02. In distant clusters, this issue becomes even more salient as a contribution is found from a dwarf starburst population (Rakos *et al.* 2000). In fact, diagrams like Figure 2 are a key tool in the interpretation of the evolution of blue galaxies since blue galaxies from mergers of high mass, gas-rich systems will contribute to the top of the luminosity function (Dressler *et al.* 1997); whereas a low mass starburst population could influence the f_B values for distant clusters than fade and disappear in present-day clusters (Rakos *et al.* 2000). In this context, Coma displays none of the high luminosity blue galaxies found in intermediate redshift clusters and the low luminosity blue galaxies have colors similar to normal star-forming galaxies, rather than starburst or AGN colors.

Lastly, the bottom panel of Figure 2 displays the run of spectrophotometric classification as a function of absolute luminosity. The distribution is not cumulative, as in the top panel, and each bin contains 20 galaxies. As expected from the low f_B values, a majority of the galaxies at high luminosities are E type. The few S types above -18 are red (early-type spirals). At fainter magnitudes, the fraction of E types declines

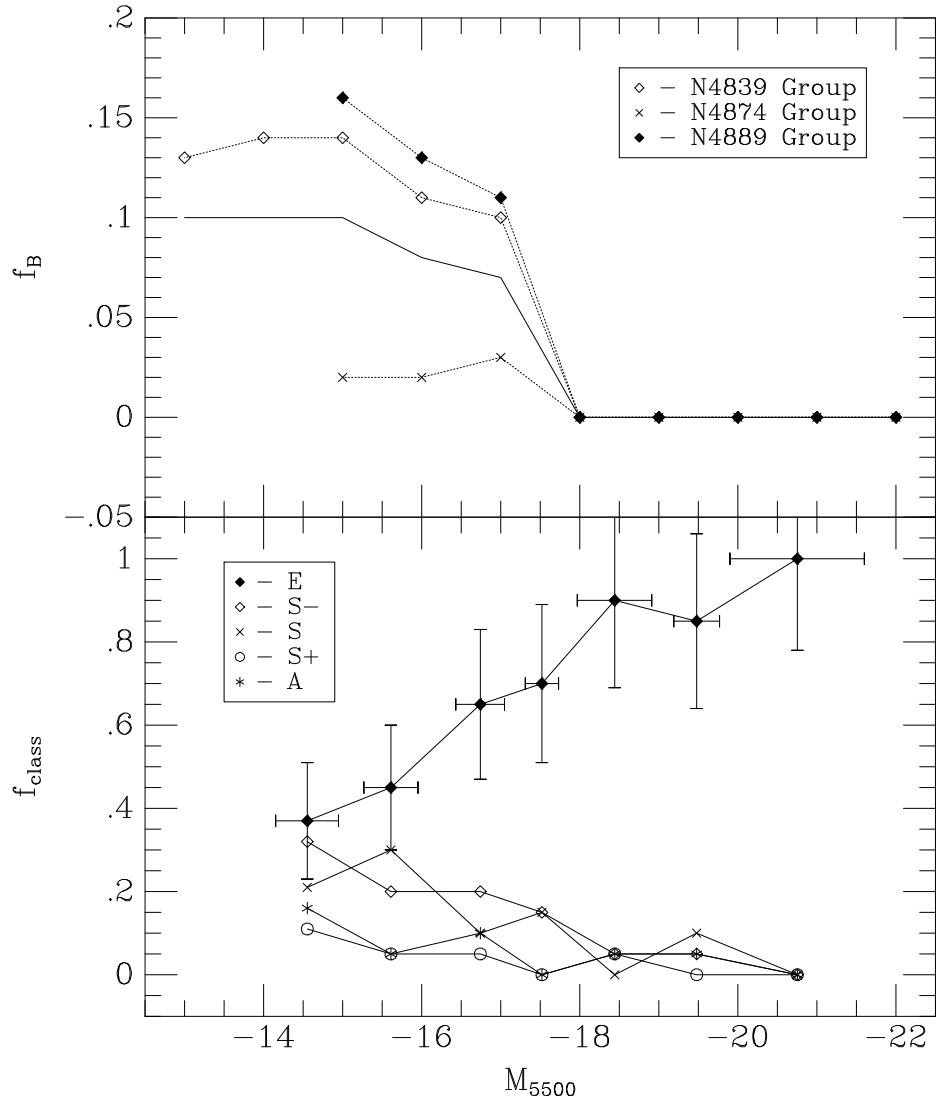


Fig. 2.— The fraction of blue galaxies, f_B , as defined by the Butcher-Oemler criteria, as a cumulative function of absolute luminosity. The NGC 4874, NGC 4889 and NGC 4839 subgroups are marked as separate symbols, the total cluster value is shown as the solid line. The trend of an increasing f_B values with decreasing luminosity is obvious for each subcluster in agreement with the result from distant clusters (Rakos *et al.* 2001). The low f_B values for NGC 4874 and NGC 4839 correlate with the existence of a cD envelope for those systems. NGC 4889, which lacks an extended envelope, has much higher f_B values indicating an environmental connection for the evolution of blue cluster galaxies. The bottom panel displays the spectrophotometric classifications in bins of 20 galaxies per magnitude. The blue galaxies are primarily due to normal spiral-like star forming galaxies. The decrease in E type as a function of luminosity is primarily a metallicity effect.

and is uniformly offset by the number of S- type of galaxies. This is primarily a metallicity effect, as the lower luminosity E type galaxies have bluer colors due to low metallicities (see next section).

3.4. Color-Magnitude Relation

One of the first discovered relationships between the global properties of galaxies and their underlying stellar populations is the color-magnitude (CM) relation (see Bower, Lucey & Ellis 1992 and reference therein). The relationship between redder galaxy color (both local and global) with increasing luminosity is well known from the era of aperture photometers (Sandage & Visvanathan 1978). The observed relationship in luminous ellipticals has largely been interpreted as reflecting a cooler RGB population (redder color) due to increased metallicity with larger galaxy masses. This has, in large part, been confirmed by numerous absorption line studies (Trager *et al.* 2000) comparing line strengths of features such as Mg₂ and Fe with dynamic measures of galaxy mass (i.e. velocity dispersion) and luminosity (a corollary for constant M/L). However, there is increasing evidence in the last few years that some of the spread in the CM relation is due to age effects or recent star formation, particularly at the low luminosity end (Poggianti *et al.* 2001).

Most CM relations found in the literature refer to the colors measured by broadband filter systems versus total luminosity; however, Worthey (1994) demonstrated that broadband colors suffer from age/metallicity degeneracy. Thus recent studies have focused on their spectral line equivalents, line strength versus magnitude (Trager *et al.* 2000). It is usually considered an obvious point that spectral line measurements are superior to colors, either narrow or broadband. However, metallicity maps into the colors of the underlying stellar population through the mean temperature of the RGB, where metal-poor stars being hotter and, therefore, bluer as compared to high metallicity stars. Line strengths directly measure these values (except where varying ratios, such as Mg/Fe, complicate matters), but stellar populations vary according to the total metallicity, Z . Our narrow band colors form a useful compromise between line studies and broadband colors through a measure of the continuum shape. In addition, spectral lines studies suffer from decreased S/N for fainter objects, (i.e. high redshift or dwarfs) whereas our narrow band system has been applied out to redshifts of 1.

The raw CM diagram, for all three Coma subclusters, is presented in Figure 3 for the metallicity color $uz - yz$ (top panel), and the continuum color $bz - yz$ (bottom panel). The colors and magnitudes are based on isophotal apertures, rather than weighted by surface brightness (unless the galaxy is less than 16 kpc in radius in which case a total aperture magnitude is used). In general, Figure 3 contains all the major features for the CM diagram for a diverse collection of galaxy types. A main ridgeline is found on the red side of the diagram that represents the sequence of those galaxies classified both morphologically and photometrically as ellipticals. As noted in our photometry of distant clusters, the CM effect is clearly visible for the $uz - yz$ color, yet the $bz - yz$ displays no correlation with luminosity. This is, in part, by design of the $uvby$ filter system where, for composite populations, the $bz - yz$ is more sensitive to contributions from hot stars (upper MS or blue HB populations) than from changes in the RGB. In contrast, the $uz - yz$ has a longer wavelength baseline and several metallicity features in the uz region to increase its sensitivity to metallicity changes.

To determine the CM relation for old, non-starforming galaxies, Figure 3 displays as solid symbols E type galaxies (see §2.3) in Coma and a sample of 47 dE galaxies from Fornax. Fitting to an iterated least-squares regression of color on magnitude produces the solid line in Figure 3 ($uz - yz = -0.036 \pm 0.005M_{5500} - 0.046 \pm 0.084$). This fit is indistinguishable in slope from the color-magnitude relation determined from distant clusters (see Rakos *et al.* 2000) out to redshifts of 0.3 with interesting variations in the zeropoint

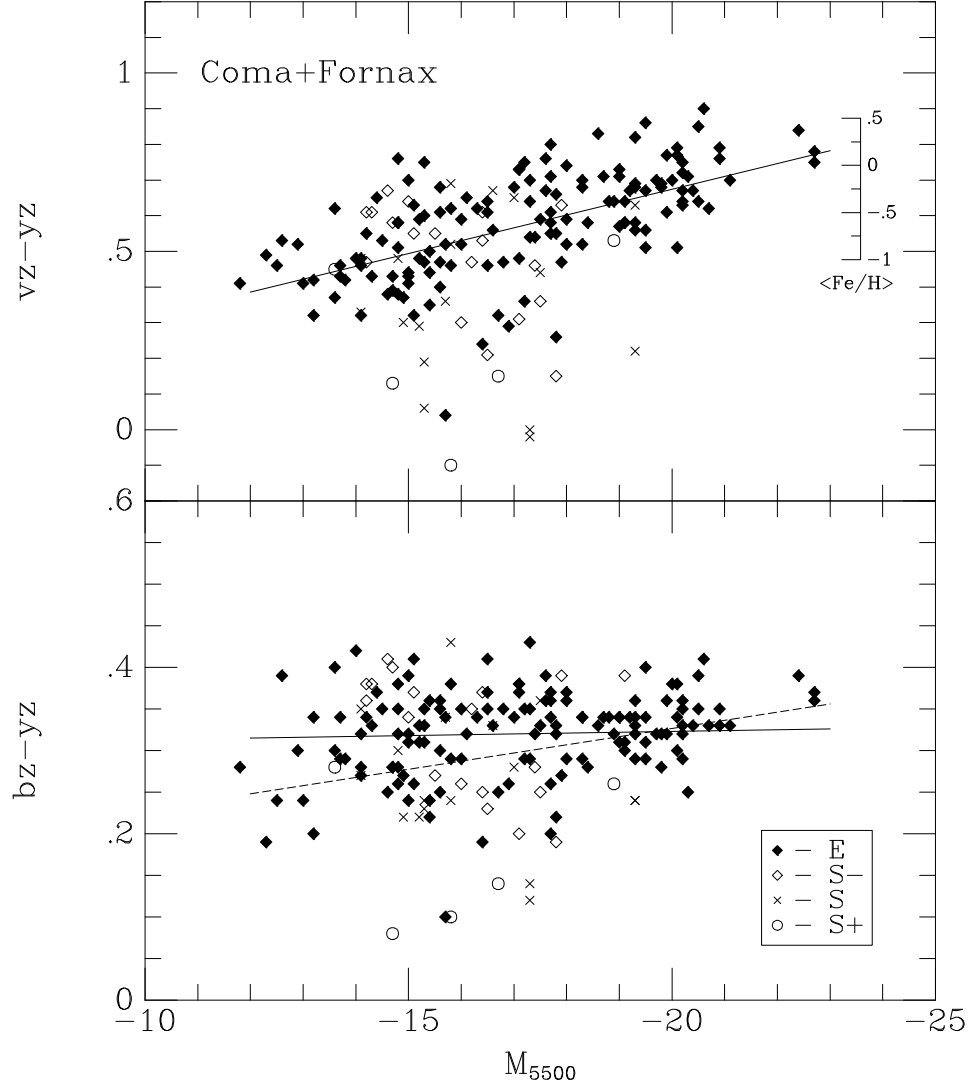


Fig. 3.— The color-magnitude diagram for all three subclusters in the Coma cluster. The top panel display the metallicity color, $vz - yz$, as a function of absolute magnitude, M_{5500} . The bottom panel displays the continuum color, $bz - yz$, as a function of apparent magnitude. Also shown is a solid line representing a robust least-squares fit to E type galaxies only. While the traditional color-magnitude relation is evident in the $vz - yz$ colors, reflecting the mass-metallicity relation for galaxies, there is no correlation visible in $bz - yz$. The expected relationship, base on multi-metallicity models, is shown as the dotted line. The lack of a relation indicates a systematic age effect.

to be discussed in a later paper. Considering only the E types, the scatter about the fit is greater than the observational error indicating that, even among galaxies without current star formation, there is a range of colors due to complicating factors such as reddening or differing mean stellar age or simply that mass and metallicity do not map, linearly, into the CM relation.

Conversion of the color-magnitude diagram into a metallicity-mass relation requires two steps, one model dependent, the other dynamical. A dynamical measurement is required to convert the luminosity of a galaxy into its mass. Lacking a companion or satellite for total dynamical mass measurements, the standard procedure is to determine a mean M/L from rotation or velocity dispersion curves and apply that value to the total luminosity of the galaxy. We lack dynamical information for most of the galaxies in our sample; however, ellipticals have an extremely narrow range in M/L and are well correlated with L (Bernardi *et al.* 2002). Thus, for our purposes, we have simply used the luminosity of the galaxies (M_{5500}) as a measure of mass with the assumption of constant M/L .

The conversion from $vz - yz$ color to metallicity (i.e. $[\text{Fe}/\text{H}]$) requires the use of spectrophotometric models. For a stellar population formed at a unique time and metallicity (a single stellar population (SSP) such as a globular cluster) the link between $vz - yz$ color and metallicity is straightforward and documented in Rakos *et al.* (2001). However, the photometry used for our study is the total luminosity for each galaxy and will be the sum of all the various stellar populations with a range of metallicities and, perhaps, ages. This is in contrast to spectroscopy where the signal is weighted by surface brightness dominated by the stars in a galaxy’s core and the assumption that a single stellar population is observed will be close to valid.

In order to correct for the contribution of stars with a range of metallicities, we have applied a very simple multi-metallicity approximation of the underlying stellar population. This method was described in Rakos *et al.* (2001) and accurately reproduces the spectroscopic measurements of metallicity with the expected colors. In brief, the underlying metallicity distribution is assumed to be Lorentzian in shape, a long tail to low metallicities and a sharp cutoff at high metallicities. A range of total metallicities is constructed by holding the lowest metal population fixed ($[\text{Fe}/\text{H}] = -2.5$) and sliding the upper cutoff from high to low. The Strömgren colors for each metallicity bin are determined by empirical calibration to globular clusters ($[\text{Fe}/\text{H}] < -1$) and spectrophotometric SSP models ($[\text{Fe}/\text{H}] > -1$, Bruzual & Charlot 2002). The resulting metallicity scale is shown as an inset in Figure 3. With this calibration, and a M/L ratio of 5 for early-type galaxies, the CM relation maps into mass-metallicity as $[\text{Z}/\text{H}] = 0.362 \log(M/M_{\odot}) - 3.736$.

In addition to plotting the CM relation for the metallicity color $vz - yz$, data also exists to test its effect on the continuum color, $bz - yz$. While the continuum color has very few direct metallicity features to produce line blanketing effects, the $bz - yz$ index is still sensitive to metallicity changes primarily due to shifts in the color of MS turnoff stars. Assuming that a correlation should exist between absolute luminosity and $bz - yz$, which is due solely to metallicity, then the Bruzual & Charlot multi-metallicity models, predicts a variation of 0.11 for the same range as the CM relationship for $vz - yz$. This model prediction is shown as a dotted line in the bottom panel of Figure 3. The data are not in agreement with this prediction despite its excellent fit to the $vz - yz$ data, although there is a tendency for the scatter to increase blueward for fainter magnitudes. In fact, the $bz - yz$ index displays no correlation with galaxy luminosity. This is not surprising since our previous work with nearby ellipticals (Schombert *et al.* 1993) and various distant clusters have all demonstrated no correlation between galaxy luminosity and the $bz - yz$ index.

There are several effects that can redden $bz - yz$ while holding $vz - yz$ relatively unchanged. For example, reddening by dust can produce the effect seen herein; however, it would require A_V between one and two to cause the observed deviation and this seems unlikely for normal cluster ellipticals based on their

IRAS luminosities. Contributions from red and blue HB stars would reproduce unusual MS turnoff colors, but again there is no expectation for such an effect. The most obvious candidate is an age effect, systematic with galaxy luminosity.

3.5. Mean Stellar Age

Another advantage to narrow band continuum colors is that a crude index of age can be assigned with the caveat that the galaxy being studied not have any current, ongoing star formation. As outlined in Rakos *et al.* (2001), a measure of the mean age of a stellar population can be found by comparing the residual in the $bz - yz$ color with the expected value based on the mean metallicity as determined by the $uz - yz$ color. This is based on the fact that the giant branch will be more sensitive to metallicity changes, whereas the turnoff stars are more sensitive to age effects.

An advance indication of the results from the residuals in $bz - yz$ can be seen in a two-color plot of the Coma E types, Fornax dwarf ellipticals and globular clusters shown in Figure 4. There appears to be a distinct population of ellipticals that share a common region of the two-color diagram with dwarf ellipticals from our Fornax work (Rakos *et al.* 2001). Also shown in Figure 4 is the 13 Gyr model from Bruzual & Charlot (2002) for a range of metallicity (convolved to our multi-metallicity models). It is clear from this comparison that low luminosity and dwarf ellipticals are too red in $bz - yz$ for their metallicity, indicating heavy reddening or an older mean stellar population. This confirms the CM relation (or lack thereof) for $bz - yz$ as low luminosity galaxies being too red for their $uz - yz$ colors.

The age indicator is the $\Delta(bz - yz)$ index, listed in Tables 1, 2 and 3 for the Coma E type galaxies. In our Fornax study, $\Delta(bz - yz)$ was determine with respect to a fiducial relationship as given by globular clusters with similar ages. Due to the much higher metallicities found for cluster ellipticals, a comparison to metal-poor globular clusters is problematic as they occupy such different regions of the two-color diagram. As an alternative method, we have calculated the residual $bz - yz$ color based on the distance in the two-color diagram from the 13 Gyr models of Bruzual & Charlot (2002). These models are an excellent fit to the red edge of the color-magnitude relation (see Figure 3), and so provide a convenient initial guess at the age of elliptical populations. Since the $\Delta(bz - yz)$ index is a relative age scheme, the choice of this fiducial zero point will not affect our results.

Figure 5 plots the $\Delta(bz - yz)$ value as a function of luminosity for the ellipticals in Coma. Also included in the Figure, for comparison, are the $\Delta(bz - yz)$ values for dwarf galaxies from Fornax (Rakos *et al.* 2001) recalculated to the Bruzual & Charlot models. The solid line is a linear least squares fit to the Coma ellipticals which yields a slope of 0.0038 ± 0.0018 with a correlation coefficient of 0.22. The probability of obtaining this or higher R by chance is 5%.

As can be seen in Figure 5, there is a clear trend for redder $\Delta(bz - yz)$ values with lower luminosity for the Coma galaxies. This implies the surprising result that low luminosity ellipticals are older than their higher mass counterparts. As calibrated to globular clusters, a change in 0.25 in $\Delta(bz - yz)$ corresponds to a change of 2 Gyrs in mean stellar age. Thus, by a magnitude of -16 , the mean age of a Coma elliptical is 2 Gyrs older than the brighter ellipticals, assumed to be 13 Gyrs by their match to the Bruzual & Charlot 13 Gyr models. This trend of older age with fainter magnitude also merges nicely into the distribution defined by Fornax dwarf ellipticals which have the reddest $\Delta(bz - yz)$ residuals.

Of course, our age indicator is a measure of mean stellar age for the entire stellar population of each

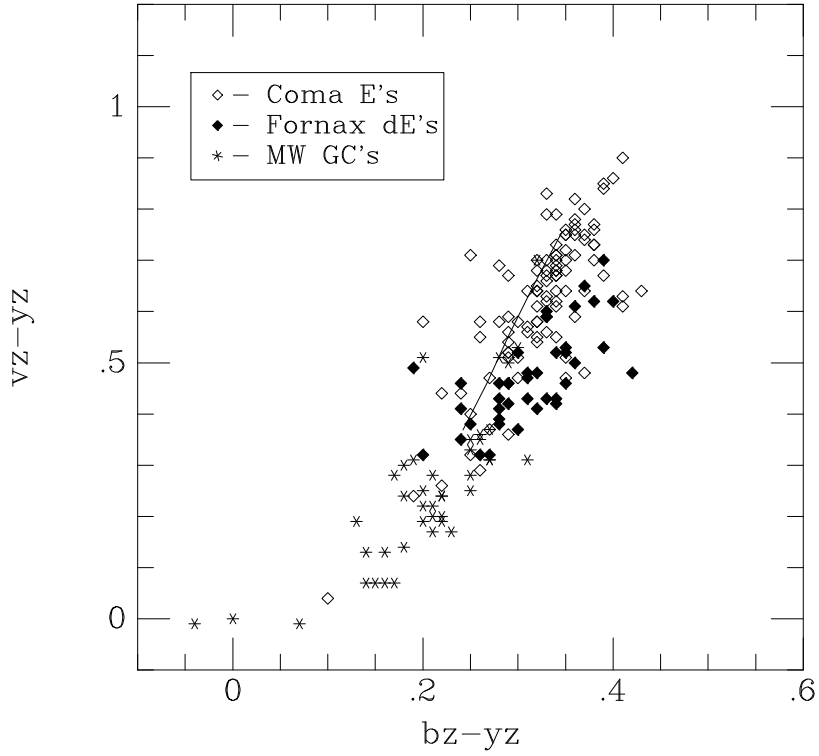


Fig. 4.— The two-color diagram for galaxies in the Coma cluster (open symbols). Also shown are dwarf ellipticals from the Fornax cluster (solid symbols, Rakos, Dominis & Steindling 2001) and globular clusters in our own Galaxy (crossed symbols, Rakos, Dominis & Steindling 2001). Also shown are the 13 Gyr models from Bruzual & Charlot (2002). A majority of the low luminosity ellipticals in this diagram display $bz - yz$ colors that are too red for their $vz - yz$, a sign of a redder turnoff population or older mean stellar age.

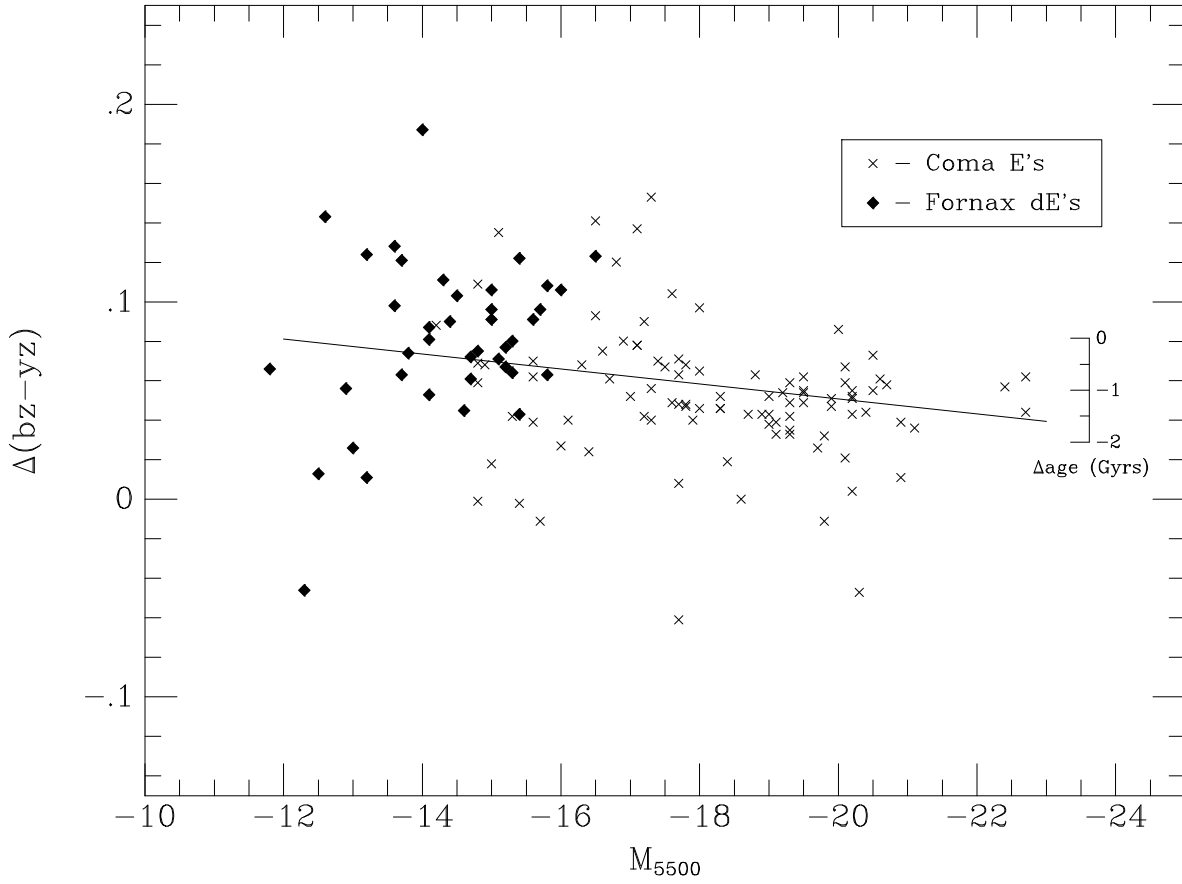


Fig. 5.— The age indicator, $\Delta(bz-yz)$, versus absolute luminosity for ellipticals in the Coma cluster (crossed symbols). Also shown are the data for dwarf ellipticals from the Fornax cluster (solid symbols, Rakos, *et al.* 2001). The dwarf ellipticals continue the trend of redder $\Delta(bz-yz)$ values (older mean stellar age) seen in the Coma data. Also shown is a rough scale for the change in mean age of the stellar population in Gyrs, relative to the dwarf elliptical sample.

galaxy as weighted by luminosity. Thus, bright ellipticals can achieve a younger mean age through various mechanisms. The simplest explanation is, of course, that bright ellipticals have later formation epochs than lower luminosity systems. Various formation scenarios invoke the late formation of massive galaxies (Kauffmann, White & Guiderdoni 1993), but usually by assembling dwarf galaxies into larger systems. If dwarf galaxies have older stellar populations, then they are poor candidates as the progenitors of massive ellipticals under this scenario. Another possibility is that dwarf and massive ellipticals have the same formation epoch, but massive ellipticals have a longer phase of initial star formation. This would produce a broad distribution of stellar ages, such that the mean age is effectively younger than dwarf ellipticals whose initial star formation timescale was brief. This also has the attractive attribute that massive ellipticals with a longer period of star formation also produce more metals and a more enriched stellar population resulting in the observed CM relation. Lastly, since the ellipticals studied herein are members of a dynamically evolved cluster, we cannot ignore the effects that mergers will have on the cluster population, particularly the upper end of the luminosity function. One explanation to the decrease in the fraction of blue galaxies for present-day clusters is that these galaxies are removed from the cluster population by mergers. The merger of galaxies with recent star formation and younger stellar populations would lower the mean stellar age as measured by our indices. And this process would preferentially occur more frequently for more massive ellipticals producing the correlation seen in Figure 5.

3.6. Environmental Effects on Metallicity and Age

While our sample does not cover a large area within the Coma cluster, we have sampled the three densest regions, those around the three brightest cluster members. This provides an opportunity to examine the run of metallicity and age with distance from the central galaxy in each subcluster. Figure 6 plots the metallicity color, $vz - yz$, as a function of radial distance from each of the brightest galaxies, NGC 4839, 4874 and 4889. There is a slight trend for decreasing metallicity with distance from the core around NGC 4874. However, much of this correlation is blurred by the large number of low luminosity galaxies nearby to the central galaxy, presumably objects on orbits decaying by dynamical friction. One concern is that the weak trend with metallicity is due to a mass segregation effect, where high mass galaxies with high metallicity occupy the subcluster cores. However, mass segregation is rarely seen in clusters (Dominguez, Muriel & Lambas 2001) and a check on absolute magnitude versus distance displays no evidence of clustering of high luminosity galaxies in the core (other than the fact that the D galaxies sit at the cluster center).

A trend of decreasing metallicity with radius is often found in the hot x-ray gas in which clusters are embedded. For example, Dupke & White (2000) find a factor of two change in the metallicity of the hot gas in Abell 496. Since the x-ray gas in clusters derives from baryonic blowout of ellipticals by galactic winds, the metallicity gradient in the gas is a relic of the metallicity gradient in the galaxy distribution from early epochs. Comparison of the current galaxy gradients versus the x-ray gradient should reveal the amount of dynamical and orbital evolution that has occurred in rich clusters.

The trend between age and cluster radius is shown in the bottom panel of Figure 6, $\Delta(bz - yz)$ versus cluster radius. There is no evidence of a radial gradient for our age indicator. This is somewhat surprising since both metallicity and age correlate with luminosity, so we would expect age to follow metallicity with respect to radial gradients. However, the correlation of age with luminosity is much weaker than metallicity and luminosity, so the relic of a cluster age gradient may be lost in the observational noise.

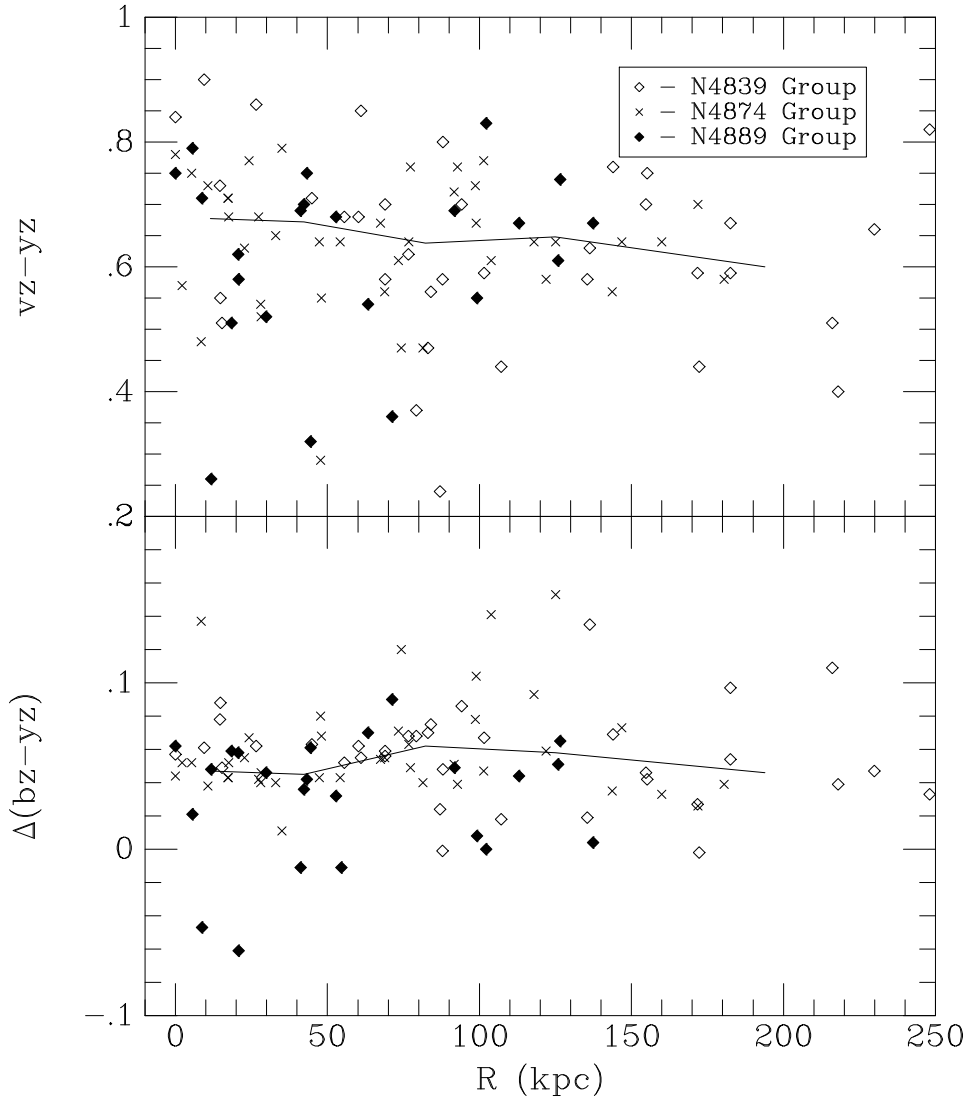


Fig. 6.— Metallicity (top panel) and mean age (bottom panel) as a function of cluster radius for the three Coma subclusters. The primary galaxies, NGC 4874, NGC 4889 and NGC 4839, form the positional center of each group. The solid lines display the running average. While there is a weak trend of decreasing metallicity with distance, there is no trend in age for any group.

4. CONCLUSIONS

We can summarize our results in two parts, pure observational results and interpretation. From the observational side, we have found that the Coma population is, unsurprisingly, rich in early-type galaxies based on their spectrophotometric classification (71%). Morphologically, these systems are predominately ellipticals and S0's as one would expect in a dense cluster like Coma. We summarize the analysis as the following:

- The fraction of blue galaxies rises slowly with decreasing galaxy luminosity, reflecting the dynamically evolved nature of the Coma system. The blue fraction is lowest in those subclusters (NGC 4874 and NGC 4839) with cD envelopes attached to the primary galaxy. It seems clear that the low blue fractions and the presence of a cD envelope are due to stripping effects, on one hand removing stars for the development of an expanded envelope while, on the other hand, halting star formation by gas stripping and lowering the number of blue, star-forming objects.
- What little blue population is found in Coma is unlike the blue population in distant clusters. It is neither bright, disk galaxies nor faint starburst objects (i.e. there are no bright, blue galaxies in Coma nor are there faint S+ type systems as found in A115 and A2283, Rakos *et al.* 2000).
- The color-magnitude relation for Coma (plus Fornax dE's) is extremely well defined for E type systems from $M_{5500} = -23$ to -13 , although the scatter is larger than the observation error. Our metallicity color, $vz - yz$, maps into mean $[\text{Fe}/\text{H}]$ such that the brightest ellipticals have luminosity weighted mean $[\text{Fe}/\text{H}]$ values of $+0.3$ while a typical low luminosity elliptical ($M_{5500} = -15$) will have a $[\text{Fe}/\text{H}]$ value of -0.8 .
- While our metallicity color ($vz - yz$) displays a strong CM relation, our continuum color ($bz - yz$) reveals no correlation with luminosity (i.e. stellar mass), although there is a bluer increase in scatter to fainter magnitudes. This is unexpected since $bz - yz$ should be weakly sensitive to metallicity through changes in the temperature of turnoff stars and suggests a counteracting age effect.
- An age effect is confirmed with our mean age indicator, $\Delta(bz - yz)$, which finds a correlation with luminosity such that bright ellipticals are about 2 Gyrs younger than dwarf ellipticals. This is a small and subtle difference, only detectable due to the wide range in luminosity for our combined Coma/Fornax sample. Since spectroscopic studies are restricted to the top of the luminosity function, it is unsurprising that this effect has been missed in previous work. This result is in agreement with the results from Terlevich & Forbes (2001) who also find that young galaxies (high mass) have high metallicities and that old galaxies (low mass) have a broad range of metallicities.

Interpretation of the above observations is problematic. A classic galactic wind model reproduces the CM relation by a simple relationship between the mass of a galaxy and its ability to retain gas by the depth of its gravitational well leading to longer, and more chemically evolved, star formation. Observations of distant clusters strongly support the metallicity interpretation for the CM relation (Kodama & Arimoto 1997). The wind model also predicts a mean age difference since more massive galaxies have a longer episode of star formation, whereas dwarf systems are extinguished quickly producing a relative older mean age. However, for traditional models (Bressan, Chiosi & Fagotto 1994), this age difference is extremely minor and the age effect for $bz - yz$ remains unresolved by a wind model.

It seems almost inescapable that the cluster environment plays an important role to the stellar populations of cluster ellipticals, especially since the most massive systems have evidence of a history of past

mergers. While the number of galaxies with blue populations is very low in present-day clusters, this was not the case in the recent past (i.e. Butcher-Oemler effect). Mergers with gas-rich, star forming galaxies would have a minor effect on the metallicity color, yet would dramatically lower the mean stellar age as estimated by the $\Delta(bz - yz)$ index. Thus, later mergers by galaxies such as spirals, with young stellar populations would explain the younger mean age of massive ellipticals, which is in agreement with the discovery of a large number of red merger systems in MS 1054-03 ($z = 0.83$, van Dokkum *et al.* 1999). This also provides a cautionary tale for the study of CM relationships in distant clusters. If an intermediate age population is visible in present-day clusters, then at moderate redshifts these same galaxies may not even be on the CM relation. For example, the scenarios developed by Kauffmann (1996) indicate that some ellipticals could enter the red envelope by redshift of 0.4 to 0.5, even though most of the stars formed at redshift greater than 2.

Lastly, our results also favor the so-called hierarchical clustering and merging scenario of galaxy formation (Kauffmann, White & Guiderdoni 1993, Kauffmann & Charlot 1998) where the massive galaxies are assembled from older, lower mass systems. Younger mean age and higher metallicities are achieved by star formation as massive ellipticals consume disk galaxies, and their cold gas, and efficiently turn this material into the bulk of their stellar populations. While the scenario to convert low metallicity, gas-rich systems into present-day red, massive ellipticals seem finely tuned to produce the correct metallicities, the difference between present-day dwarf and giant elliptical ages (about 2 Gyrs, see Figure 5) does match the predictions of the hierarchical models (see Kauffmann & Charlot 1998 Figure 3). However, the data only supports a conclusion that massive systems are younger, whether that is from assembly history or an extended star formation history is unclear. The narrow range of metallicity for high mass galaxies argues for a uniform star formation history in high mass systems. The range in metallicities for younger systems implies a more stochastic process where the weaker gravitational fields are more susceptible to environmental effects such as cluster ram pressure stripping.

The authors wish to thank NOAO and Steward Observatory for granting telescope time for this project. One of us (K. Rakos) gratefully acknowledges the financial support from the Austrian Fonds zur Foerderung der wissenschaftlichen Forschung.

REFERENCES

- Adami, C., Nichol, R., Mazure, A., Durret, F., Holden, B. & Lobo, C. 1998, *A&A*, 334, 765
Anthony-Twarog, B. & Twarog, B. 2000, *AJ*120, 3111
Bell, R. & Gustafsson, B. 1978, *A&A*34, 229
Bernardi, M., Alonso, M., da Costa, L., Willmer, C., Wegner, G., Pellegrini, P., Rite, C. & Maia, M. 2002, *AJ*, 123, 2159
Bernstein, G., Nichol, R., Tyson, J., Ulmer, M. & Wittman, D. 1995, *AJ*, 110, 1507
Bower, R., Lucey, J. & Ellis, R. 1992, *MNRAS*, 254, 589
Bressan, A., Chiosi, C. & Fagotto, F. 1994, *ApJS*, 94, 63
Bruzual, A. & Charlot, S. 2002, in prep
Burns, J., Roettiger, K., Ledlow, M. & Klypin, A. 1994, *ApJ*, 427, L87
Butcher, H. & Oemler, A. 1984, *ApJ*, 285, 426

- Caldwell, N. & Rose, J. 1998, AJ, 113, 492
- Caldwell, N., Rose, J., Sharples, R., Ellis, R. & Bower, R. 1993, AJ, 106, 473
- Colles, M. & Dunn, A. 1996, ApJ, 458, 435
- Chaboyer, B., Sarajedini, A. & Armandroff, T. 2000, AJ120, 3102
- De Propriis, R., Pritchett, C., Harris, W. & McClure, R. 1995, ApJ, 450, 534
- van Dokkum, P., Franx, M., Fabricant, D., Kelson, D. & Illingworth, G. 1999, ApJ, 520, 95
- Dominguez, M., Muriel, H. & Lambas, D. 2001, AJ, 121, 1266
- Dressler, A. 1980, ApJ, 236, 351
- Dressler, A., Oemler, A., Couch, W., Smail, I., Ellis, R., Barger, A., Butcher, H., Poggianti, B. & Sharples, R. 1997, ApJ, 490, 577
- Ellis, R., Colliess, M., Broadhurst, T., Heyl, J. & Glazebrook, K. 1996, MNRAS, 280, 235
- Dupke, R. & White, R. 2000, ApJ, 537, 123
- Ferguson, H. & Binggeli, B. 1994, ARA&A, 6, 67
- Ferguson, H. & Sandage, A. 1991, AJ, 101, 765
- Fitchett, M. & Webster, R. 1987, ApJ, 317, 653
- Geller, M. & Beers, T. 1982, PASP, 94, 421
- Grebel, E. & Richtler, T. 1992, *a*253, 359
- Grebel, E. 1998, *Highlights of Astronomy*, ed. J. Andersen (Dordrecht:Kluwer), Vol. 11, p.125
- Hamuy, M., Suntzeff, N., Heathcote, A., Walker, A., Gigoux, P. & Phillips, M. 1994, PASP, 106, 566
- Henry, J., Henrikson, M., Charles, P. & Thorstensen, J. 1981, ApJ, 243, L137
- Hilker, M. 2000, *a*, 355, 994
- Kauffmann, G., White, S. & Guiderdoni, B. 1993, MNRAS, 254, 201
- Kauffmann, G. 1996, MNRAS, 281, 487
- Kauffmann, G. & Charlot, S. 1998, MNRAS, 294, 705
- Kodama, T. & Arimoto, N. 1997, A&A, 320, 41
- Kuntschner, H., Lucey, J., Smith, R., Hudson, M. & Davies, R. 2001, MNRAS, 323, 615
- Massey, P. & Gronwall, C. 1990, ApJ358, 344
- Melbourne, J., Sarajedini, A., Layden, A., & Martins, D. 2000, AJ, 120, 3127
- Metcalf, N., Godwin, J. & Peach, J. 1994, MNRAS, 267, 431
- Oemler, A. 1992 in *Clusters and Superclusters of Galaxies*, ed. A.C. Fabian (Dordrecht:Kluwer), 666
- Poggianti, B., Bridges, T., Mobasher, B., Carter, D., Doi, M., Iye, M., Kashikawa, N., Komiyama, Y., Okamura, S., Sekiguchi, M., Shimasaku, K., Yagi, M., Yasuda, N 2001, ApJ, 562, 689
- Rakos, K., Schombert, J. & Kreidl, T. 1991, ApJ, 377, 382
- Rakos, K. & Schombert, J. 1995, ApJ, 439, 47
- Rakos, K., Maindl, T. & Schombert, J. 1996, ApJ, 466, 122
- Rakos, K., Odell, A. & Schombert, J. 1997, ApJ, 490, 194

- Rakos, K., Schombert, J., Odell, A. & Steindling, S. 2000, *ApJ*, 540, 715
- Rakos, K., Dominis, D., & Steindling, S. 2001, *ã369*, 750
- Rakos, K., Schombert, J., Maitzen, H., Prugovecki, S. & Odell, A. 2001, *AJ*, 121, 1974
- Richtler T., 1989, *ã211*, 199
- Salaris, M. & Weiss, A. 1998, *ã*, 335, 943
- Sandage, A. & Visvanathan, N. 1978, *ApJ*, 223, 707
- Sarajedini, V., Green, R., Griffiths, R. & Ratnatunga, K. 1996, *ApJ*, 471, L15
- Schombert, J. 1987, *ApJS*, 64, 643
- Schombert, J. 1988, *ApJ*, 328, 475
- Schombert, J., Hanlan, P., Barsony, M. & Rakos, K. 1993, *AJ*, 106, 923
- Secker, J., & Harris, W. 1996, *ApJ*, 469, 623
- Secker, J., Harris, W. & Plummer, J. 1997, *PASP*109, 1377
- Smith, R.M., Driver, S.P., Phillips, S. 1997, *MNRAS*287, 415
- Steindling, S., Brosch, N. & Rakos, K. 2001, *ApJS*132, 19
- Terlevich, A. & Forbes, D. 2002, *MNRAS*, in press.
- Thompson, L. & Gregory, S. 1993, *AJ*, 106, 2197
- Trager, S., Faber, S., Worthey, G. & Gonzalez, J. 2000, *AJ*, 120, 165
- Worthey, G. 1994, *ApJS*, 418, 947

Table 1. NGC 4889 Group

object	R.A. (J2000)	Dec.	$uz - vz$	$bz - yz$	$vz - yz$	mz	m_{5500}	M_{5500}	[Fe/H]	$\Delta(bz - yz)$	Class
a001	195.11765	27.97243	0.57	0.25	0.71	+0.21	14.5	-20.3	-0.15	-0.047	E
a002	195.11595	27.95587	0.63	0.28	0.69	+0.13	15.0	-19.8	-0.22	-0.011	E
a004	195.10321	27.92628	1.14	0.26	0.55	+0.03	17.1	-17.7	-0.75	+0.008	E
a005	195.10493	27.94904	1.24	0.10	0.04	-0.16	19.1	-15.7	-2.68	-0.011	E
a008	195.09177	28.04706	0.59	0.29	0.67	+0.09	14.6	-20.2	-0.30	+0.004	E
a009	195.07054	28.06402	0.34	0.24	0.63	+0.15	15.5	-19.3	A
a010	195.07803	28.00925	0.79	0.32	0.54	-0.10	17.4	-17.4	-0.79	+0.070	E
a011	195.07297	27.98753	0.78	0.20	0.58	+0.18	17.1	-17.7	-0.64	-0.061	E
a012	195.06839	27.96748	0.76	0.30	0.51	-0.09	14.7	-20.1	-0.90	+0.059	E
a013	195.07330	27.95535	0.71	0.33	0.70	+0.04	13.7	-21.1	-0.18	+0.036	E
a014	195.07784	27.93681	0.19	0.26	0.53	+0.01	15.9	-18.9	A+
a016	195.04771	27.90973	0.06	0.14	0.15	-0.13	18.1	-16.7	S+
a017	195.03104	27.95817	0.60	0.39	0.63	-0.15	16.9	-17.9	S-
a018	195.03491	27.95486	1.20	0.35	0.75	+0.05	17.6	-17.2	+0.01	+0.042	E
a020	195.03368	27.97692	0.87	0.37	0.75	+0.01	12.1	-22.7	+0.01	+0.062	E
a021	195.06104	28.04119	0.71	0.32	0.61	-0.03	14.9	-19.9	-0.52	+0.051	E
a023	195.02196	28.02441	0.62	0.39	0.58	-0.20	15.7	-19.1	S-
a025	195.02632	28.00390	0.66	0.32	0.68	+0.04	15.0	-19.8	-0.26	+0.032	E
a026	195.01826	27.98746	0.75	0.33	0.62	-0.04	14.1	-20.7	-0.49	+0.058	E
a028	195.00418	27.94552	0.64	0.20	0.31	-0.09	17.7	-17.1	S-
a029	194.99791	27.94050	1.17	0.29	0.36	-0.22	17.6	-17.2	-1.47	+0.090	E
a030	194.98627	27.93001	0.68	0.34	0.69	+0.01	15.5	-19.3	-0.22	+0.049	E
a031	194.95891	27.91228	0.56	0.37	0.74	+0.00	16.8	-18.0	-0.03	+0.065	E
a032	194.95872	27.92476	0.60	0.33	0.83	+0.17	16.2	-18.6	+0.31	+0.000	E
a033	194.99225	27.95422	0.98	0.25	0.32	-0.18	18.1	-16.7	-1.62	+0.061	E
a034	194.97449	27.97064	0.33	0.36	0.44	-0.28	17.3	-17.5	S
a035	194.94420	27.97405	0.78	0.34	0.79	+0.11	14.7	-20.1	+0.16	+0.021	E
a036	194.95183	27.98291	0.83	0.22	0.26	-0.18	17.0	-17.8	-1.85	+0.048	E
a037	194.94472	27.99217	1.15	0.29	0.52	-0.06	16.8	-18.0	-0.86	+0.046	E
a038	194.94385	28.00025	0.72	0.25	0.36	-0.14	17.3	-17.5	S-
a039	194.98268	28.03465	0.76	0.33	0.67	+0.01	14.4	-20.4	-0.30	+0.044	E

Table 2. NGC 4874 Group

object	R.A. (J2000) Dec.		$uz - vz$	$bz - yz$	$vz - yz$	mz	m_{5500}	M_{5500}	[Fe/H]	$\Delta(bz - yz)$	Class
b041	194.93370	27.86699	1.01	0.30	0.58	-0.02	15.7	-19.1	-0.64	+0.039	E
b042	194.93550	27.88941	0.66	0.28	0.46	-0.10	17.4	-17.4	S-
b043	194.95770	27.90875	0.85	0.38	0.73	-0.03	17.7	-17.1	-0.07	+0.078	E
b044	194.93430	27.91231	0.82	0.35	0.72	-0.02	14.6	-20.2	-0.11	+0.051	E
b045	194.92560	27.92468	0.79	0.34	0.67	-0.01	15.6	-19.2	-0.30	+0.054	E
b046	194.93370	27.95802	0.76	0.31	0.57	-0.05	15.8	-19.0	-0.68	+0.052	E
b047	194.93179	27.99426	0.90	0.31	0.56	-0.06	15.3	-19.5	-0.71	+0.055	E
b048	194.90781	28.00071	1.12	0.27	0.47	-0.07	16.9	-17.9	-1.05	+0.040	E
b049	194.90910	27.98681	0.85	0.32	0.64	+0.00	15.9	-18.9	-0.41	+0.043	E
b050	194.88609	27.98334	0.78	0.32	0.64	+0.00	14.6	-20.2	-0.41	+0.043	E
b051	194.91730	27.96798	0.74	0.34	0.71	+0.03	16.1	-18.7	-0.15	+0.043	E
b052	194.91460	27.95369	0.67	0.34	0.73	+0.05	15.8	-19.0	-0.07	+0.038	E
b053	194.89160	27.94679	0.76	0.38	0.77	+0.01	14.7	-20.1	+0.08	+0.067	E
b054	194.89600	27.93476	0.95	0.26	0.29	-0.23	17.9	-16.9	-1.73	+0.080	E
b055	194.89720	27.90611	0.90	0.41	0.61	-0.21	18.3	-16.5	-0.52	+0.141	E
b056	194.90710	27.90736	0.72	0.36	0.77	+0.05	14.9	-19.9	+0.08	+0.047	E
b057	194.87750	27.88416	0.92	0.35	0.64	-0.06	14.3	-20.5	-0.41	+0.073	E
b058	194.88310	27.92120	0.89	0.35	0.47	-0.23	18.0	-16.8	-1.05	+0.120	E
b059	194.87151	27.94231	0.86	0.32	0.65	+0.01	18.7	-16.1	-0.37	+0.040	E
b060	194.87910	27.95481	1.01	0.37	0.48	-0.26	17.7	-17.1	-1.02	+0.137	E
b061	194.87421	27.95642	0.83	0.36	0.75	+0.03	14.6	-20.2	+0.01	+0.052	E
b062	194.88370	28.00196	0.59	0.35	0.47	-0.23	18.6	-16.2	S-
b063	194.90390	28.01830	0.37	0.28	0.65	+0.09	17.8	-17.0	A
b064	194.88049	28.04687	0.83	0.32	0.70	+0.06	15.1	-19.7	-0.18	+0.026	E
b065	194.86890	28.04081	0.89	0.31	0.64	+0.02	15.7	-19.1	-0.41	+0.033	E
b066	194.86819	28.01925	0.55	0.25	0.53	+0.03	18.4	-16.4	S-
b067	194.87300	28.00630	0.53	0.24	0.19	-0.29	19.5	-15.3	S
b068	194.86031	27.99831	0.70	0.34	0.64	-0.04	16.0	-18.8	-0.41	+0.063	E
b069	194.85381	27.99657	0.74	0.34	0.61	-0.07	17.1	-17.7	-0.52	+0.071	E
b070	194.85561	27.97312	0.82	0.33	0.68	+0.02	15.5	-19.3	-0.26	+0.042	E
b071	194.85500	27.96792	0.82	0.34	0.71	+0.03	15.8	-19.0	-0.15	+0.043	E
b072	194.85500	27.93464	0.83	0.32	0.55	-0.09	17.0	-17.8	-0.75	+0.068	E
b073	194.84689	27.91965	0.78	0.36	0.76	+0.04	17.2	-17.6	+0.04	+0.049	E
b075	194.84650	27.91174	0.75	0.35	0.76	+0.06	13.9	-20.9	+0.04	+0.039	E
b076	194.84860	27.89026	0.74	0.23	0.21	-0.25	18.3	-16.5	S-
b077	194.84340	27.89692	0.77	0.32	0.58	-0.06	15.5	-19.3	-0.64	+0.059	E
b078	194.83299	27.88579	0.77	0.29	0.56	-0.02	15.5	-19.3	-0.71	+0.035	E
b079	194.80960	27.89528	0.87	0.43	0.64	-0.22	17.5	-17.3	-0.41	+0.153	E
b080	194.81371	27.89891	1.13	0.37	0.64	-0.10	18.3	-16.5	-0.41	+0.093	E
b081	194.79680	27.98085	0.82	0.19	0.15	-0.23	17.0	-17.8	S-
b082	194.83121	27.96808	0.92	0.34	0.68	+0.00	17.8	-17.0	-0.26	+0.052	E
b083	194.83859	27.97356	0.88	0.29	0.52	-0.06	16.5	-18.3	-0.86	+0.046	E
b084	194.83141	27.97346	1.18	0.29	0.54	-0.04	17.5	-17.3	-0.79	+0.040	E
b085	194.81261	27.97074	0.91	0.33	0.63	-0.03	14.6	-20.2	-0.45	+0.055	E

Table 2—Continued

object	R.A. (J2000)	Dec.	$uz - vz$	$bz - yz$	$vz - yz$	mz	m_{5500}	M_{5500}	[Fe/H]	$\Delta(bz - yz)$	Class
b086	194.80341	27.97701	0.86	0.33	0.79	+0.13	13.9	-20.9	+0.16	+0.011	E
b087	194.81870	27.98257	0.45	0.34	0.64	-0.04	19.8	-15.0	A-
b088	194.79649	28.00965	0.92	0.39	0.67	-0.11	17.2	-17.6	-0.30	+0.104	E
b089	194.89841	27.95914	0.88	0.36	0.78	+0.06	12.1	-22.7	+0.12	+0.044	E

Table 3. NGC 4839 Group

object	R.A. (J2000) Dec.		$uz - vz$	$bz - yz$	$vz - yz$	mz	m_{5500}	M_{5500}	[Fe/H]	$\Delta(bz - yz)$	Class
c090	194.29520	27.56129	0.61	0.37	0.61	-0.13	18.4	-16.4	S-
c091	194.30000	27.58170	0.59	0.23	0.06	-0.40	19.5	-15.3	S
c092	194.34760	27.55026	0.82	0.33	0.59	-0.07	17.3	-17.5	-0.60	+0.067	E
c093	194.35710	27.54647	0.90	0.38	0.70	-0.06	14.8	-20.0	-0.18	+0.086	E
c094	194.37691	27.54337	0.77	0.37	0.80	+0.06	17.1	-17.7	+0.19	+0.048	E
c095	194.38860	27.54876	0.64	0.14	-0.02	-0.30	17.5	-17.3	S
c096	194.39600	27.56802	0.67	0.41	0.63	-0.21	19.7	-15.1	-0.45	+0.135	E
c097	194.42931	27.57742	0.75	0.34	0.70	+0.02	16.5	-18.3	-0.18	+0.046	E
c098	194.44240	27.57191	0.94	0.38	0.76	+0.00	20.0	-14.8	+0.04	+0.069	E
c099	194.46870	27.57764	0.83	0.35	0.75	+0.05	19.5	-15.3	+0.01	+0.042	E
c100	194.46181	27.53464	0.77	0.26	0.30	-0.22	18.8	-16.0	S-
c101	194.45911	27.52099	0.54	0.22	0.29	-0.15	19.6	-15.2	S
c102	194.35130	27.49843	0.90	0.39	0.84	+0.06	12.4	-22.4	+0.35	+0.057	E
c103	194.36481	27.53753	0.69	0.34	0.62	-0.06	18.5	-16.3	-0.49	+0.068	E
c104	194.31120	27.51770	0.22	0.28	0.45	-0.11	21.2	-13.6	A+
c105	194.28650	27.50831	0.59	0.38	0.47	-0.29	20.6	-14.2	S-
c106	194.29530	27.52918	0.76	0.35	0.68	-0.02	19.2	-15.6	-0.26	+0.062	E
c107	194.26750	27.52678	0.78	0.34	0.68	+0.00	16.5	-18.3	-0.26	+0.052	E
c108	194.30521	27.54821	0.54	0.40	0.58	-0.22	20.1	-14.7	S-
c109	194.23320	27.48264	0.59	0.38	0.61	-0.15	20.5	-14.3	S-
c110	194.23340	27.48046	0.33	0.33	0.67	+0.01	18.2	-16.6	A
c111	194.23241	27.46325	0.69	0.35	0.70	+0.00	17.5	-17.3	-0.18	+0.056	E
c112	194.26241	27.46611	0.50	0.22	0.30	-0.14	19.9	-14.9	S
c113	194.26199	27.46325	0.65	0.32	0.58	-0.06	20.0	-14.8	-0.64	+0.059	E
c114	194.28900	27.46725	0.92	0.39	0.85	+0.09	14.3	-20.5	+0.38	+0.055	E
c115	194.28430	27.49088	0.85	0.34	0.55	-0.13	20.6	-14.2	-0.75	+0.088	E
c116	194.34039	27.47550	0.82	0.36	0.71	-0.01	17.1	-17.7	-0.15	+0.063	E
c117	194.34200	27.47079	0.52	0.41	0.67	-0.15	20.2	-14.6	A-
c118	194.35060	27.46414	0.47	0.35	0.48	-0.22	20.7	-14.1	S
c119	194.40070	27.48488	0.88	0.40	0.86	+0.06	15.3	-19.5	+0.42	+0.062	E
c120	194.39940	27.49360	0.92	0.41	0.90	+0.08	14.2	-20.6	+0.57	+0.061	E
c121	194.44971	27.49450	0.42	0.24	0.52	+0.04	19.0	-15.8	S
c122	194.46181	27.49094	0.96	0.38	0.73	-0.03	17.7	-17.1	-0.07	+0.078	E
c123	194.47690	27.49059	0.89	0.29	0.51	-0.07	15.3	-19.5	-0.90	+0.049	E
c124	194.46851	27.47190	0.53	0.10	-0.10	-0.30	19.0	-15.8	S+
c125	194.45790	27.47672	0.51	0.34	0.36	-0.32	19.1	-15.7	S
c126	194.47279	27.45355	1.07	0.26	0.58	+0.06	20.0	-14.8	-0.64	-0.001	E
c127	194.46770	27.44369	0.84	0.24	0.44	-0.04	19.8	-15.0	-1.17	+0.018	E
c128	194.48730	27.44220	0.73	0.12	0.00	-0.24	17.5	-17.3	S
c129	194.44150	27.42925	0.75	0.28	0.58	+0.02	16.4	-18.4	-0.64	+0.019	E
c130	194.45219	27.45402	0.97	0.19	0.24	-0.14	18.4	-16.4	-1.92	+0.024	E
c131	194.43280	27.46159	0.64	0.27	0.55	+0.01	19.3	-15.5	S-
c132	194.40370	27.46332	0.40	0.08	0.13	-0.03	20.1	-14.7	S+
c133	194.41180	27.45552	0.83	0.33	0.56	-0.10	18.2	-16.6	-0.71	+0.075	E

Table 3—Continued

object	R.A. (J2000)	Dec.	$uz - vz$	$bz - yz$	$vz - yz$	mz	m_{5500}	M_{5500}	[Fe/H]	$\Delta(bz - yz)$	Class
c134	194.30270	27.45796	0.82	0.27	0.37	-0.17	19.9	-14.9	-1.43	+0.068	E
c135	194.24809	27.45603	0.76	0.30	0.47	-0.13	19.2	-15.6	-1.05	+0.070	E
c136	194.25661	27.37173	0.88	0.36	0.82	+0.10	15.5	-19.3	+0.27	+0.033	E
c137	194.26350	27.38813	0.75	0.35	0.51	-0.19	20.0	-14.8	-0.90	+0.109	E
c138	194.30119	27.38709	0.93	0.25	0.40	-0.10	19.2	-15.6	-1.32	+0.039	E
c139	194.29480	27.40521	0.81	0.34	0.67	-0.01	15.3	-19.5	-0.30	+0.054	E
c140	194.29660	27.40131	0.64	0.37	0.55	-0.19	19.7	-15.1	S-
c141	194.29410	27.41943	0.53	0.27	0.33	-0.21	20.7	-14.1	S
c142	194.30521	27.41071	0.72	0.29	0.59	+0.01	18.8	-16.0	-0.60	+0.027	E
c143	194.30679	27.40899	0.45	0.30	0.48	-0.12	20.0	-14.8	S
c144	194.33990	27.39591	0.53	0.36	0.61	-0.11	20.6	-14.2	S-
c145	194.35190	27.38834	0.40	0.43	0.69	-0.17	19.0	-15.8	A
c146	194.35580	27.40462	0.66	0.24	0.22	-0.26	15.5	-19.3	S
c147	194.35880	27.40519	0.74	0.36	0.59	-0.13	16.8	-18.0	-0.60	+0.097	E
c148	194.40610	27.41045	0.94	0.22	0.44	+0.00	19.4	-15.4	-1.17	-0.002	E
c149	194.48770	27.38107	0.89	0.33	0.66	+0.00	17.0	-17.8	-0.34	+0.047	E

Table 4. Cluster Population Fractions

	NGC 4889		NGC 4874		NGC 4839		Total	
E	23	(74%)	40	(83%)	35	(58%)	98	(71%)
S-	4	(13%)	5	(10%)	8	(13%)	17	(12%)
S	1	(3%)	1	(2%)	11	(18%)	13	(9%)
S+	1	(3%)	0	(0%)	2	(3%)	3	(2%)
A	2	(6%)	2	(4%)	4	(7%)	8	(6%)
	31	(22%)	48	(35%)	60	(43%)	139	
blue	5	(16%)	1	(2%)	8	(13%)	14	(10%)
red	26	(84%)	47	(98%)	52	(87%)	125	(90%)